Wireless Power Transfer

ARTICLE

Open Access

https://doi.org/10.48130/wpt-0025-0007

Wireless Power Transfer **2025**, 12: e011

Parameter identification method for a wireless power transfer system based on the Improved Northern Goshawk Optimization Algorithm

Zhen Guo, Shuang Chen*, Minghao Ye, Jiqiu Nai, Haitao Yu, Zhaodong Li, Hailong Zhang, Yanbing Tian and Min Zhang

College of Information and Control Engineering, Qingdao University of Technology, Qingdao 266520, Shandong, China

* Corresponding author, E-mail: chen_shuang824@126.com

Abstract

This paper proposes a mutual inductance and load parameter identification method using an Improved Northern Goshawk Optimization (INGO) Algorithm after pulse frequency modulation (PFM), and validates the effectiveness of the proposed parameter identification method through a maximum efficiency tracking approach. One of the most challenging aspects of wireless power transfer (WPT) technology for electric vehicles is the variation in the magnetic coupling coefficient between the two coils due to inaccurate parking positions and differences in height. First, a steady-state circuit model of an SS-type compensation network and pulse frequency modulation strategy was established to determine the correlation between system parameters. The INGO was then introduced to convert the parameter identification problem into an optimization problem, enabling the identification of load and mutual inductance parameters. Finally, the proposed identification method was experimentally validated, and the maximum efficiency tracking of the proposed WPT system was achieved through a Sepic impedance matching circuit. The results show that the identification method can maintain high accuracy even under coil displacement and load variation conditions.

Citation: Guo Z, Chen S, Ye M, Nai J, Yu H, et al. 2025. Parameter identification method for a wireless power transfer system based on the Improved Northern Goshawk Optimization Algorithm. *Wireless Power Transfer* 12: e011 https://doi.org/10.48130/wpt-0025-0007

Introduction

Wireless power transmission (WPT) technology has been a hot research topic in the last decade due to its flexibility, low maintenance, and safety[1]. These systems have formed the basis for various industrial applications and interdisciplinary fields, such as wireless charging for electric vehicles[2,3], wireless motors[4–6], wireless lighting[7], wireless energy-on-demand[8], wireless power encryption[9], and wireless power trading[10]. It is widely used in the medical field, consumer electronics, household appliances, and electric vehicles[11,12].

There are multiple parameter variations in the application of WPT and this paper aims to study wireless charging in electric vehicles. When the deviation of the parking position of the electric vehicle and the difference in the height of the vehicle chassis will affect the change of the coupling coefficient and lead to the change of mutual inductance[13,14], as well as the equivalent impedance of the vehicle's energy storage battery will increase with the charging time during the charging process, which will lead to the decrease of the charging efficiency[15]. The parameter identification technique is beneficial to the development of appropriate control strategies to maintain the stability and efficiency of the system.

At present, some scholars have carried out related research around the problem of identifying the load and mutual inductance parameters of WPT systems. When the system does not use a modulation strategy, some researchers use a primary-side open-ended capacitor to ensure that the receiver-side reflected impedance at three frequencies can form the imaginary part of the input impedance, and then the voltage and current are collected to complete the identification of the system parameters[16]. Some researchers use the method of switching circuits to short-circuit the compensation network at the receiving end, and then obtain the phase information of the output voltage and current of the inverter by the method of sweeping to realise the identification of the parameters[17]. Some researchers propose a parameter identification method based on impedance matching, which parameterises different circuit models according to loads of different natures, obtains the parameter relationship between the transmitter and the load, and completes the parameter identification[18]. Each of these methods requires the addition of extra circuitry, which increases the cost and is only applicable to parameter identification for one topology.

In terms of different modulation strategies applied, some researchers proposes a WPT load parameter identification method by DC input current and phase shift angle. Due to the phase shift control used in the controller, the phase shift angle can be easily calculated, and the identification of the parameters can be accomplished simply by collecting the input current at the transmitter side[19]. A parameter identification method based on pulse density modulation (PDM) is proposed, in which a series of interharmonics are obtained by varying the sequence of the PDM, a system of equations is constructed using the simple harmonic waves, and finally, the load and mutual inductance are estimated using the least-squares approximation[20]. However, both PSC and PDM have a non-negligible problem, that is, PSC has high switching loss and is not easy to achieve zero voltage switching (ZVS); PDM can easily achieve ZVS, but the output fluctuation is large. Moreover, the identification method is very complicated due to the application of the modulation method.

Intelligent algorithm technology has been developing rapidly in recent years, and researchers have begun to apply AI algorithms to WPT systems to solve the problem of mutual inductance and load identification[21]. In this paper, a parameter identification method based on the Improved Northern Goshawk Optimization (INGO) Algorithm is proposed, which converts parameter identification into an optimal problem, and accurate identification of mutual inductance and load can be accomplished by collecting the output current of the inverter, and the proposed identification method is applied to the WPT system that incorporates the pulse frequency

control strategy, and achieves the maximum efficiency tracking of the WPT system through impedance matching.

Compared to existing methods, the main contributions of this paper are as follows:

An Improved Northern Goshawk Optimization (INGO) Algorithm is proposed, which introduces an optimal value guidance strategy, a subtraction optimizer, and Cauchy mutation to enhance the global convergence speed and the ability to escape local optima. This improvement makes the parameter identification process more efficient and accurate, especially under conditions of load variation, and coil misalignment.

The proposed method integrates the parameter identification process with the Pulse Frequency Modulation (PFM) strategy, which effectively reduces switching frequency and switching losses while suppressing output fluctuations. Compared to traditional Phase Shift Control (PSC) and Pulse Density Modulation (PDM), PFM simplifies the control strategy and reduces the complexity of parameter identification.

Beyond parameter identification, this paper achieves maximum efficiency tracking through a Sepic impedance matching circuit, ensuring that the system maintains maximum transmission efficiency even under load variations and coil misalignment.

The proposed method significantly reduces hardware complexity and system cost by eliminating the need for additional circuits or complex control strategies, as required in traditional methods[16, 17].

We begin by analyzing the system topology and the principle of operation, followed by an introduction to the basic principles of the PFM modulation strategy. Additionally, the calculation method for the output current of the inverter circuit after applying the PFM modulation strategy is presented. The relationship between mutual inductance and the basic parameters of the circuit is derived, and the load and mutual inductance are identified using the measured current on the transmitter side. Finally, the conditions required for the Sepic circuit to achieve the maximum efficiency of the system are derived.Next, an INGO algorithm is proposed, which enhances the algorithm's ability to escape local optima and accelerates the speed of global convergence. The entire identification process is described in detail. The feasibility of the proposed INGO algorithm for parameter identification is then verified through simulation and experimental results.In conclusion, the effectiveness of the method and its practical applications are summarized.

System architecture and modeling analysis

System model analysis

Due to its advantages such as simple structure, strong stability, and ease of control, the SS-type topology is widely used in electric vehicles and medical electronics[22]. Therefore, this paper analyzes and discusses the SS-type topology. Figure 1 shows the equivalent circuit diagram of the SS-type topology.

U_{dc} is the DC voltage input to the system. S1~S4 is a full-bridge inverter circuit composed of four mosfets, which can generate an approximate square-wave input AC voltage U_{in} by alternating the conduction of two groups of switching tubes, and I_p is the input AC current after inversion. L_p and L_s are the self-inductances of the transmission coils on the transmitter and receiver, respectively. C_p and C_s are the resonant compensation capacitors on both sides. R_p and R_s are the equivalent series resistances on both sides. $R_e = 8R_L/\pi^2$ represents the equivalent resistance of the load and rectifier circuit on the receiver side, while the load R_L varies with the charging time. The mutual inductance M between the transmission coils is $M = k(L_pL_s)^{1/2}$. Where k is the coupling coefficient between the coils, when the coils are offset k changes resulting in a change in the M.

Since the reactive power can be minimised when the system operates at the resonant frequency, the operating frequency ω of the system can be set to approximate the resonant frequencies ω_p and ω_s. The operating frequency ω is given by Eqn (1).

$$\omega \approx \omega_P \approx \omega_S \approx \frac{1}{\sqrt{L_p C_p}} \approx \frac{1}{\sqrt{L_s C_s}} \tag{1}$$

At this point, the WPT system circuit equation is:

$$\begin{cases} U_{in} = \left(R_P + jX_{P\_n}\right) I_p + j\omega M I_s \\ 0 = j\omega M I_p + (R_s + R_e + jX_{s\_n}) I_s \end{cases} \tag{2}$$

where, X_{p_n} and X_{s_n} are the reactances under the excitation of the nth harmonic voltage at the output of the inverter on the transmitter and receiver sides, respectively.

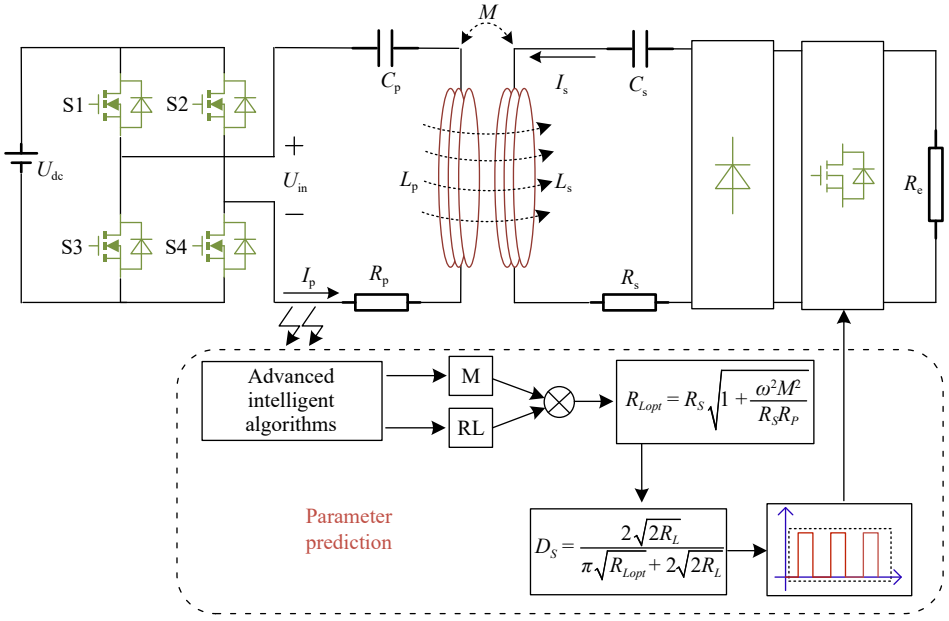

Fig. 1 SS type topology structure input by inverter.

$$\begin{cases} X_{p\_n} = n\omega L_p - \dfrac{1}{n\omega C_p} \\ X_{s\_n} = n\omega L_s - \dfrac{1}{n\omega C_s} \end{cases} \tag{3}$$

The input impedance can be expressed as $Z_{in_n} = a_n + jb_n$, where:

$$\begin{cases} a_n = R_p + \dfrac{n^2\omega^2 M^2 (R_s + R_e)}{(R_s + R_e)^2 + X_{s\_n}^2} \\ b_n = X_{p\_n}^2 - \dfrac{n^2\omega^2 M^2 X_{s\_n}}{(R_s + R_e)^2 + X_{s\_n}^2} \end{cases} \tag{4}$$

The transmission efficiency of the system is obtained from Eqn (2) as:

$$\eta = \frac{\omega^2 M^2 R_e}{(R_s + R_e)\left(R_p (R_s + R_e) + \omega^2 M^2\right)} \tag{5}$$

To achieve maximum efficiency transmission we need to optimise the load resistance. So the efficiency η can be calculated as a differential with respect to R_e. When the system satisfies the maximum efficiency transmission, the optimum load resistance is:

$$R_{eopt} = R_S \sqrt{1 + \frac{\omega^2 M^2}{R_S R_P}} \tag{6}$$

Pulse frequency modulation

To enhance the efficiency and stability of WPT systems and meet the demands under various operating conditions, modulation strategies are often implemented in the full-bridge inverter circuit on the transmitter side. Pulse Frequency Modulation (PFM) has become a focus of research due to its alternating modulation at two different frequencies and its ability to easily achieve soft switching. Compared to traditional Phase Shift Control (PSC), PFM effectively reduces switching frequency and switching losses. Furthermore, compared to Pulse Density Modulation (PDM), PFM not only reduces switching frequency but also effectively suppresses output fluctuations. Figure 2 illustrates the theoretical modulation waveform of PFM.

In PFM, the system alternates modulation between two different frequencies, f and $f/3$. Here, N_1 represents the number of square waves at the switching frequency f, and N_2 represents the number of square waves at the switching frequency $f/3$. The PFM control of the inverter output is essentially a piecewise function, which can be expressed in its Fourier series form as:

$$U_{in}(t) = \begin{cases} \dfrac{4E}{\pi} \sum\limits_{n_F}^{\infty} \dfrac{\sin[(2n_F - 1)\omega_{2n-1} t]}{2n_F - 1} & \omega_{2n-1} = \dfrac{\omega}{2n-1} \\ \dfrac{4E}{\pi} \sum\limits_{n_F}^{\infty} \dfrac{\sin[(2n_F - 1)\omega_{2n+1} t]}{2n_F - 1} & \omega_{2n-1} = \dfrac{\omega}{2n+1} \end{cases} \tag{7}$$

where, $\omega_{2n\pm1}$ are the modulating angular frequencies of the two segmented output voltages, and by selecting the output vectors generated by two neighbouring $(2n \pm 1)$ harmonics, the target vector with the minimum output fluctuation can be synthesized. The WPT system is driven by the odd harmonic segments since the odd harmonic frequencies of the two segmented function outputs are equal to the system operating frequency. The characteristics of the system are determined by its fundamental components, so the average Fourier series expansion of the fundamental components of the output voltage of the PFM inverter is as follows[23]:

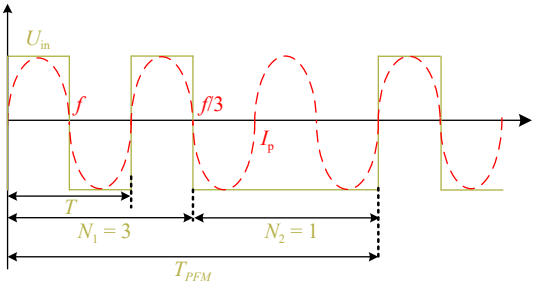

Fig. 2 PFM theoretical modulation waveform.

$$\begin{aligned} U_{in\_1}(t) &= \frac{\alpha n_1}{\alpha n_1 + (1-\alpha) n_2} \frac{4U}{n_1 \pi} \sin(n_1 \omega_{2n-1} t) \\ &\quad + \frac{(1-\alpha) n_1}{\alpha n_1 + (1-\alpha) n_2} \frac{4U}{n_2 \pi} \sin(n_2 \omega_{2n+1} t) \\ &= \frac{1}{\alpha n_1 + (1-\alpha) n_2} \frac{4U}{\pi} \sin(\omega t) \end{aligned} \tag{8}$$

where, $n_1 = 2n - 1$, $n_2 = 2n + 1$. $\alpha = N_1/(N_1 + N_2)$ is the control variable duty cycle factor of PFM. The transmitter side current can be expressed as:

$$i_p(t) = \frac{U_{in\_1}(t)}{Z_{in\_n}} = I_n \sin(\omega t) \tag{9}$$

where, I_n is the peak value of the nth harmonic of the inverter output current:

$$\begin{aligned} I_n &= \frac{1}{\alpha n_1 + (1-\alpha) n_2} \frac{4U}{\pi |Z_{in\_n}|} \\ &= \frac{1}{\alpha n_1 + (1-\alpha) n_2} \frac{4U}{\pi \sqrt{a_n^2 + b_n^2}} \end{aligned} \tag{10}$$

By bringing Eqn (3) into Eqn (9), one can solve for:

$$M = \frac{1}{\omega} \sqrt{X_{p\_1} X_{s\_1} - R_p R_e + \sqrt{\left(\frac{4U}{\pi I_n}\right)^2 (R_e^2 + X_{s\_1}^2) - (X_{p\_1} R_e + X_{s\_1} R_p)^2}} \tag{11}$$

The initial steady state period after the system enters the steady state for the first time is denoted as T_{PFM_0}, then $T_{PFM\_0} = nT_{PFM}$. By collecting the current at the moment of T_{PFM_0} on the transmitter side and constructing the fitness function with the current obtained from the computation of Eqn (10), the identification of the variations of the parameters M and R_L can be carried out in the algorithm.

Maximum efficiency tracking

Impedance matching technology can be mainly divided into two implementation methods: passive and active. The passive impedance matching method uses combinations of capacitors and inductors in series and parallel to transform the load impedance, ensuring that the imaginary part of the equivalent impedance is zero while the real part matches the system's optimal load. However, this method can result in complex circuit structures when attempting to match arbitrary loads. Moreover, in practical applications, the load resistance typically varies dynamically, and the parameters of passive impedance matching networks are difficult to adjust in real-time, making it challenging to adapt to these dynamic changes and limiting the system's efficiency optimization capabilities. In contrast to passive impedance matching, the active impedance matching method can dynamically adjust the secondary-side equivalent impedance by adjusting the duty cycle of a DC-DC converter, without the need to change system component parameters. This effectively overcomes the limitations of passive matching and optimizes system efficiency.

As shown in Table 1, the Sepic converter offers significant advantages in impedance matching applications within wireless charging systems due to its wide input-output voltage range, stable voltage polarity, efficient power transfer, and good current matching capabilities. Therefore, this paper selects the Sepic converter to implement the system's maximum efficiency tracking, and its topology is shown in Fig. 3.

The input and output voltages of the Sepic circuit are related to the equivalent resistance as follows:

Table 1. Comparison of five basic DC-DC converters

Characteristic	Sepic	Boost	Buck-Boost	Cuk	Zeta
The range of R_{eq}	0 ~ +∞	0 ~ R_L	0 ~ +∞	0 ~ +∞	0 ~ +∞
The polarity of U_S/U_o	Same	Same	Reverse	Reverse	Reverse
Conversion efficiency	Higher	higher	medium	medium	medium
Input current continuity	Continuous	Discontinuous	Discontinuous	Continuous	Continuous
Cost	medium	Lower	medium	higher	higher

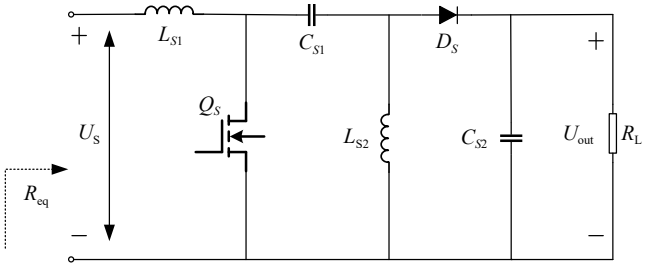

Fig. 3 Receiver added to the Sepic circuit.

$$\frac{U_S{}^2}{R_{eq}} = \frac{U_{out}{}^2}{R_L} \tag{12}$$

Assuming that the duty cycle of switching tube Q_S in the Sepic circuit is D_S, then:

$$U_{out} = \frac{t_{on}}{t_{off}} U_E = \frac{t_{on}}{T - t_{on}} U_E = \frac{D_S}{1 - D_S} U_E \tag{13}$$

The relationship between the equivalent resistance R_{eq} and the duty cycle D_S in the Sepic circuit is given by:

$$R_{eq} = (\frac{1 - D_S}{D_S})^2 R_L \tag{14}$$

The system receiver impedance R_e with duty cycle D_S can be derived as:

$$R_e = \frac{8}{\pi^2} \times \left(\frac{1 - D_S}{D_S}\right)^2 R_L \tag{15}$$

For a determined static WPT system has a unique best load value, so that $R_e = R_{eopt}$, the system load resistance R_L and duty cycle D_S when the system is at the point of maximum transmission efficiency is obtained as:

$$D_S = \frac{2\sqrt{2R_L}}{\pi\sqrt{R_{eopt}} + 2\sqrt{2R_L}} \tag{16}$$

Mutual sense recognition based on improvement of the Northern Goshawk Optimization Algorithm

The Northern Goshawk Optimization Algorithm is a population-based optimisation algorithm that is conceived through the hunting strategy of the Northern Goshawk[24]. The hunting of the Northern Goshawk consists of two phases: prey recognition and attack and chase and escape, in the first phase, after recognising the prey it moves towards it at high speed, and in the second phase it hunts the prey with a short tail chase process. The Algorithm simulates the hunting process of the Northern Goshawk.

Introducing an optimal value guidance strategy

In the first stage of the prey escape process of NGO, when $F_{P_i} < F_i$ NGO is randomly picking a hawk to guide the whole population for position updates, which can make the whole population for fast convergence but also leads to the blindness of the Optimization. In this paper, we improve to use the optimal value to guide the position update. The improved formula is as follows, where x_{best} is the best value of each generation.

$$x_{i,j} + q(x_{best} - Ix_{i,j}), F_{G_i} < F_i \tag{17}$$

Introduction of subtraction algorithm of optimizer

In the first stage of the NGO, during the prey escape process, when $F_{G_i} > F_i$, the Subtraction Optimizer Algorithm is introduced[25]. By using the Subtraction Optimizer Algorithm for position updates, it not only avoids the blindness and randomness of the NGO but also leverages the global particle update capability of the Subtraction Optimizer, thereby reducing the probability of the original NGO getting trapped in local optima. The updated position update formula for the INGO Algorithm is as follows:

$$x_{new1,i,j} = \begin{cases} x_{i,j} + q(x_{best} - Ix_{i,j}) & F_{G_i} < F_i \\ x_{i,j} = x_{i,j} + \vec{q}\frac{1}{N}\sum_{K=1}^{N}(x_i - {}_v x_k) & F_{G_i} \geqslant F_i \end{cases} \tag{18}$$

From Eqn (18), it can be seen that the subtractive optimiser will synthesise the global position which is constantly updated, which, to some extent, enhances the likelihood of the algorithm jumping out of the local optimum and accelerates the global convergence.

Adding probability factors for Cauchy variation

Adding a certain probability factor for Cauchy mutation in the 2nd stage of the NGO's Pursuit and Escape. The Cauchy variation formula is as follows:

$$x_{newbest} = x_{best} + x_{best} Cauchy\,(0,1) \tag{19}$$

Dynamic updating of position based on upper and lower bounds

In the 2nd stage of the NGO pursuit and escape, certain probability factors are added for Cauchy variation, and upper and lower limits are introduced for gradual reduction. This allows the NGO to dynamically shrink the target range as the number of iterations increases, accelerating the convergence ability of the Algorithm. The second stage of the improved formula is as follows:

$$x_{new1,i,j} = \begin{cases} x_{new2,i,j} = x_{best} + x_{best} Cauchy(0,1) & rand < \sigma \\ x_{new2,i,j} = x_{i,j} + \dfrac{r(2s-1)(ub-lb)}{t} & rand > \sigma \end{cases} \tag{20}$$

where, Cauchy(0,1) is the Cauchy variation and σ is the variation factor, when $rand < \sigma$, the Cauchy variation is used. t is the number of iterations, and it can be seen that when $rand > \sigma$, the INGO gradually reduces the search range with the number of iterations, which accelerates the convergence of the Algorithm.

Figure 4 shows the experimental plot of the proposed Algorithms in this paper in comparison with other Optimizations. Comparison with Subtractive Algorithm of Optimization (SAO) Sparrow Search Algorithm (SSA), Dung Beetle Optimization (DBO) Golden Jackal Optimization (GJO), and the original NGO shows the superiority of the INGO proposed in this paper in terms of speed of convergence as well as in terms of comparison of error.

Since particle swarm optimization (PSO) and genetic algorithms (GA) have been studied for a long time, this paper compares the proposed improved Northern Goshawk Algorithm (INGO) with more

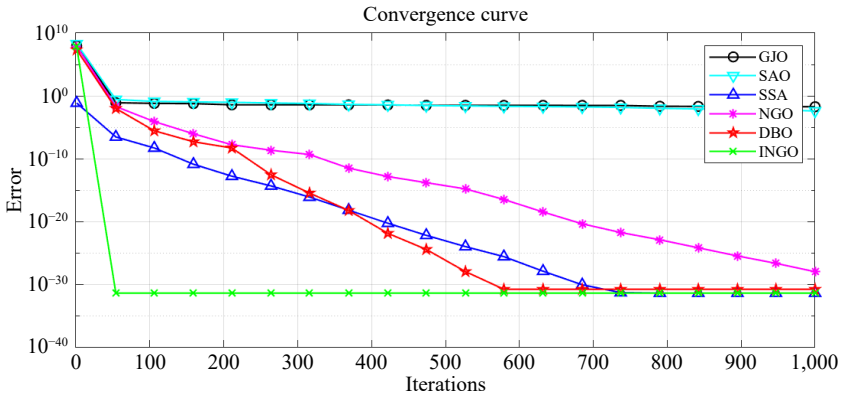

Fig. 4 Comparison of the performance of the optimization proposed in this paper with the remaining several optimizations.

recent optimization algorithms, such as the Sparrow Search Algorithm (SSA) and the Scarab Beetle Algorithm (SAO), which are currently popular in the optimization field. Compared to other artificial intelligence algorithms, the INGO algorithm achieves a better balance between computational efficiency and recognition accuracy. INGO introduces several enhancement features, including optimal value guidance strategy, subtraction optimizer, and Cauchy mutation, all of which improve global exploration and local optimization. Although these features slightly increase the computational cost per iteration, INGO compensates for this by requiring fewer iterations. This makes INGO faster and more accurate, particularly in parameter identification problems in WPT systems. Table 2 shows a comparison between INGO and other algorithms with the same population size and iteration count. INGO typically converges in 100 iterations with an average recognition error of 1.2%, while DBO and SSA require 600 and 750 iterations with average errors of 1.5%. Although GJO and SAO converge quickly, their recognition accuracy is poor, with an average error of 3.8%.

Figure 5 shows a flowchart of the implementation of the proposed improved northern goshawk parameter identification method, which is described as follows:

(1) Input the system fixed parameter values (U_{dc}, L_P, L_S, C_P, C_S, R_P, R_S), and parameterise the actual system model to get the transmitter side current $i(T_{PFM\_0})$ and measure the system $i(T_{PFM\_0})_{real}$ during steady state operation.

(2) The initial population is generated according to the basic theory of the NGO. In this paper, the initial population size is set to 50, the load identification range is [0, 100 Ω], and the mutual sensing identification range is [0, 50 μH].

(3) The adaptation function is calculated by the error between the theoretical and actual values of the transmitter side currents and the result is used to reflect the similarity between the identified parameters and the actual parameters. The fitness function $f(R_L,M)$ is as follows:

$$f(R_L,M) = \sqrt{[i(T_{PFM\_0}) - i(T_{PFM\_0})_{real}]^2 + [i(T_{PFM\_0}+T_{PFM}) - i(T_{PFM\_0}+T_{PFM})_{real}]^2} \quad (21)$$

(4) Starting the execution of IGNO, updating the position of the northern Goshawk in the first and second phases. To determine whether the maximum number of iterations has been reached, or a predefined error is satisfied.

(5) The load optimal solution is obtained and solved to the M through Eqn (11), completing the whole identification process.

Experiment analysis and discussion

To verify the effective recognition results and feasibility of the proposed recognition method, we built the SS-WPT experimental platform as shown in Fig. 6, and the system parameters are shown in Table 3.

Table 2. Comparison with other algorithms in parameter identification.

Algorithm	Avg. error (%)	Iterations	Computation time (t/s)
INGO	1.5%	87	50
SAO	3.8%	50	30
SSA	1.5%	49	110
DBO	1.5%	581	80
GJO	3.8%	726	30

The detailed geometric shapes and dimensions of the transmitter-side and receiver-side coils are shown in Fig. 7a. Compared to fully wound planar spiral coils, the hollow planar spiral coils have a higher quality factor. The coil is made of 300 strands of Leeds wire with a total cross-sectional area of 2.35 mm^2, 19 turns of dense winding, the outer diameter of the coil is 200 mm, the inner diameter of the coil is 140 mm, and the transmission distance is 70 mm. Ferrite strips, as well as an aluminium plate, are affixed on the coil to facilitate the increase of the coupling coefficient and the realization of the magnetic field shielding function, and the distribution of the magnetic field is shown in Fig. 7b.

The actual measured values of the system load R_L and mutual inductance M are 30 Ω and 34.97 μH, respectively, and the primary current is collected as the input condition of the Optimization, at this time, the circuit waveform is shown in Fig. 8.

In view of the mutual inductance parameter changes due to coil offset during system operation, this paper analyses six sets of data without loss of generality, with the horizontal offset parameters to be identified as shown in Table 4 and the vertical offset parameters to be identified as shown in Table 5.

Figure 9a shows the comparison between the actual and predicted values of mutual inductance when the receiving coil is horizontally shifted. Figure 9b shows the predicted parameter errors of the proposed method in this paper when the receiving coil is horizontally shifted, and the predicted error value is a maximum 3.039%, and a minimum 0.1% when the mutual inductance M is varied from 34.97 to 22.356 μH. Fixing the horizontal offset to zero and adjusting the position of the receiving and transmitting coils longitudinally along the z-axis, Fig. 10a shows the curve of the variation between the actual and predicted values of the mutual inductance M when the distance between the receiving and transmitting coils varies from 50 to 110 mm. The error between its predicted and actual values is given in Fig. 10b. It can be seen that the maximum error in the mutual inductance M prediction in terms of coil distance variation is 3.3% and the minimum error is 0.7%.

Because the load parameters may change during the operation of the system, this paper analyses the five groups of data without loss

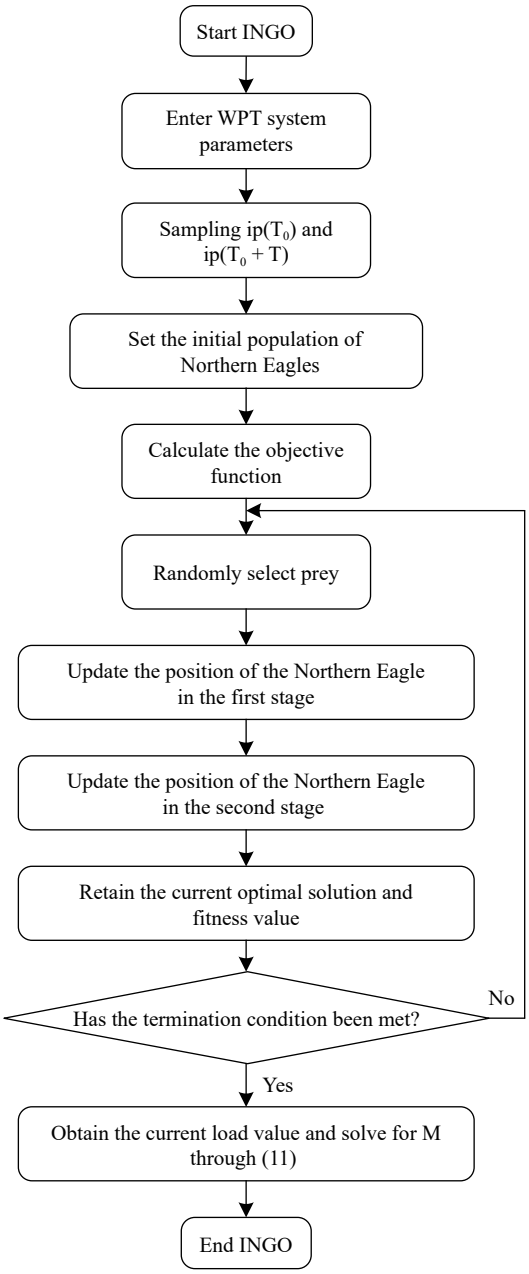

Fig. 5 INGO recognition flowchart.

of generality, and the actual values of the four groups of parameters to be identified are shown in Table 6.

Figure 11a shows the comparison between the system identification value and the predicted value when the load changes, when the R_L changes, the maximum error and the minimum error of the system identification are shown in Fig. 11b, which are 3.1% and 0.69%, respectively. So no matter the system changes during the charging process of load or sudden sensing, the error of the identification method proposed in this paper can be controlled within 3.5%, and the parameter identification ability is high.

The recognition effectiveness of the NGO algorithm is compared with that of the INGO algorithm under the same recognition parameters. The values of load RL and mutual inductance M are set to be 30 Ω, 34.97 μH, and 28.954 μH, respectively. The two algorithms are used to perform recognition six times and their errors are averaged. Figure 12a depicts the comparison of the average error between the INGO algorithm and the recognition effect of the NGO algorithm, and it can be seen that after the introduction of the optimal bootstrap value

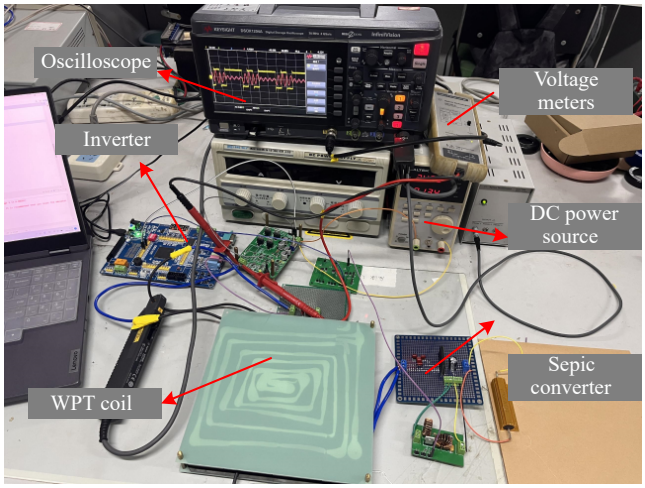

Fig. 6 Experimental model of the proposed WPT system.

Table 3. Design parameters and specifications.

Items	Value
DC input voltage (U_{dc})	24 V
Transmitter compensated capacitance (C_P)	16.5 nF
Transmitter coil inductance (L_P)	152.87μH
Receiver compensated capacitance (C_S)	16.49 nF
Receiver inductances (L_S)	153.6 μH
Sepic inductances (L_{S1})	34.6 μH
Sepic inductances (L_{S2})	33.4 μH
Sepic compensated capacitance (C_{S1})	47 μF
Sepic output capacitance (C_{S2})	2,200 μF
Fundamental switching frequency (f)	100 kHz

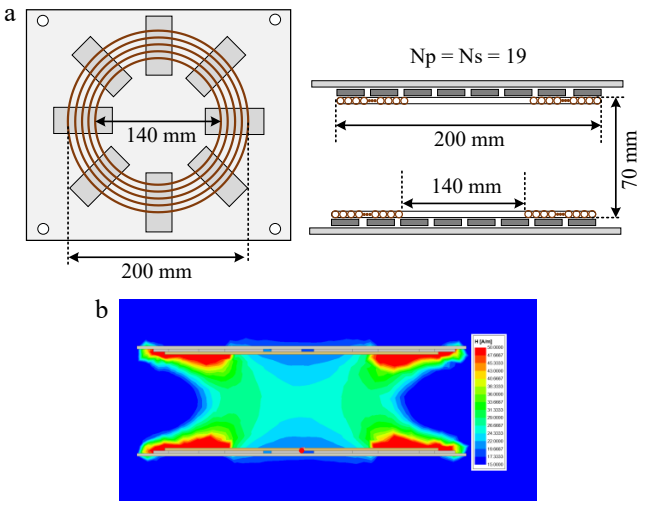

Fig. 7 (a) Transmitter and receiver side coil geometry. (b) Coil magnetic field distribution.

strategy and the subtraction optimiser algorithm, the INGO algorithm has a significant improvement in the search ability, and the accuracy is better than that of the NGO algorithm. Figure 12b shows the computation time comparison between the two algorithms in the six recognition processes, which shows that compared with the NGO algorithm, the INGO algorithm has greatly improved the convergence speed of the algorithm, reduced the number of iterations, and reduced the computation time to a great extent after the introduction of Cauchy's mutation and the introduction of the upper and lower bounds for the dynamic updating of the position.

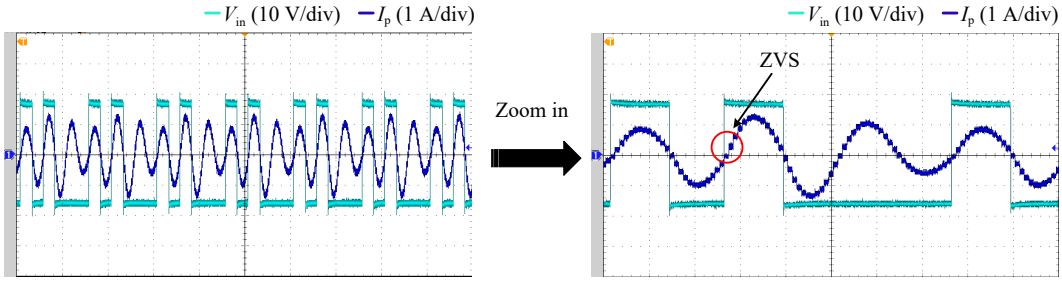

Fig. 8 Measured waveform of the PFM transmitter.

Table 4. Identification parameter value of mutual inductance parameter change.

0ffset (cm)	R (Ω)	M-x (μH)
1	30	34.14
2	30	33.01
3	30	30.95
4	30	28.41
5	30	25.47
6	30	22.35

Table 5. Identification parameter value of mutual inductance parameter change.

0ffset (cm)	R (Ω)	M-z (μH)
−2	30	53.72
−1	30	43.49
1	30	28.95
2	30	23.93
3	30	19.17
4	30	16.47

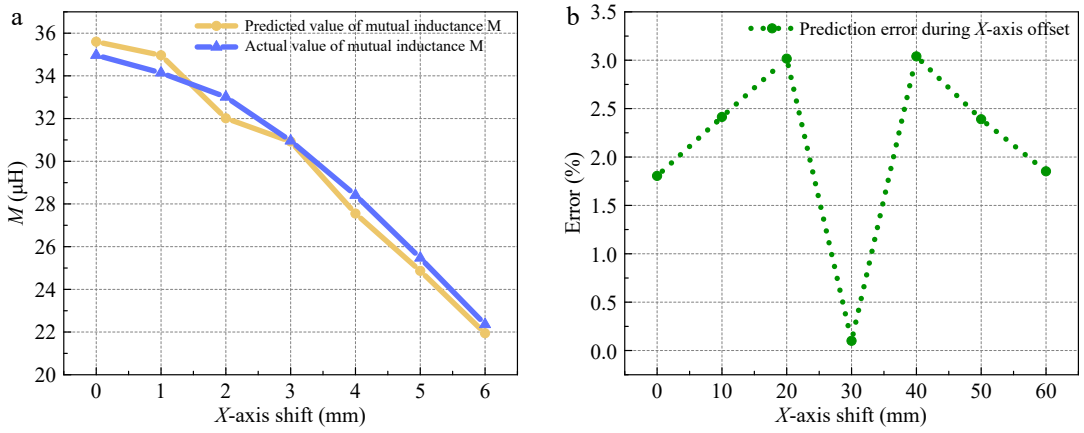

Fig. 9 Comparison between the actual value of mutual sensing and the recognition result at lateral offset. (a) Comparison of identified and actual values. (b) Error.

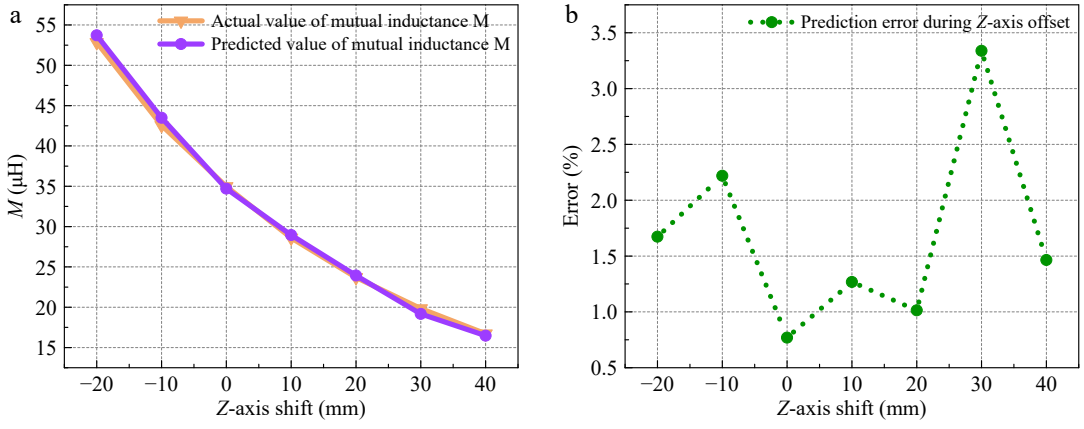

Fig. 10 Comparison between the actual value of mutual sensing and the recognition result at longitudinal offset. (a) Comparison of identified and actual values. (b) Error.

After applying the proposed scheme, the optimal equivalent load at the current level of offset can be calculated by using the mutual inductance parameters obtained from the algorithm identification using Eqn (6). Figure 13 illustrates the relationship between the optimal equivalent load corresponding to when the coil is horizontally offset and the actual load of the system. By adjusting the duty cycle of the switching tube of the Sepic circuit, the current equivalent resistance is transformed into the optimal equivalent resistance value, which can achieve the maximum efficiency of the system transmission. The duty cycle can also be calculated by Eqn (16)

Table 6. Identification of parameter values for load parameter variations.

Case	R (Ω)	M (μH)
1	10	34.97
2	30	34.97
3	50	34.97
4	70	34.97
5	90	34.97

when the system load is changed to achieve maximum efficiency. Figure 14 shows the comparison of the system transmission efficiency when the coil level is offset and when the load is changed with or without using the impedance matching circuit, from which it can be seen that the system always works at maximum efficiency after using the impedance matching circuit, which verifies the effectiveness of the Sepic impedance converter.

$$U_{\text{out}} = \frac{N_1 + N_2}{N_1 + 3N_2} U_{dc} \tag{22}$$

The relationship between the output voltage and the input voltage of the system modulated by the pulse frequency is given by Eqn (22), and the different output voltages required by the load can be satisfied by adjusting the values of N_1 and N_2. At this time the system operating frequency is[26]:

$$f_{PFM} = \frac{N_1 + N_2}{N_1 + 3N_2} f \tag{23}$$

From Eqn (23), it can be seen that the switching frequency can be effectively reduced by the PFM system. The switch can be effectively turned on/off before the current crosses the zero point to achieve soft switching. Figure 15 illustrates the comparison of system transmission efficiency when two different modulation strategies are applied.

To highlight the differences between the method proposed in this paper and other tuning methods, Table 7 presents a comparative analysis of several features. Compared with other research strategies, this approach simplifies the control method, reduces the identification complexity, and minimizes the circuit size[16,17,27]. In comparison with the study by Guo et al.[19], although the identification complexity is similar, the method proposed here achieves

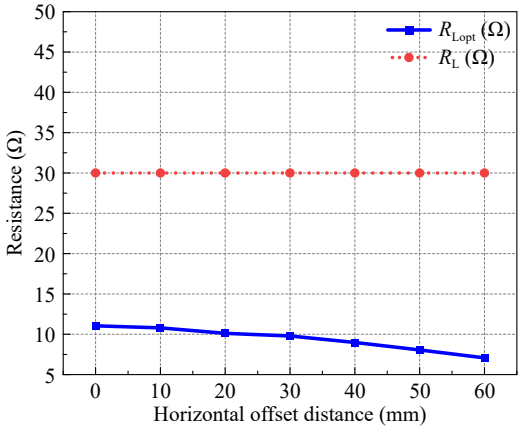

Fig. 13 Equivalent resistance calculated from recognised mutual inductance.

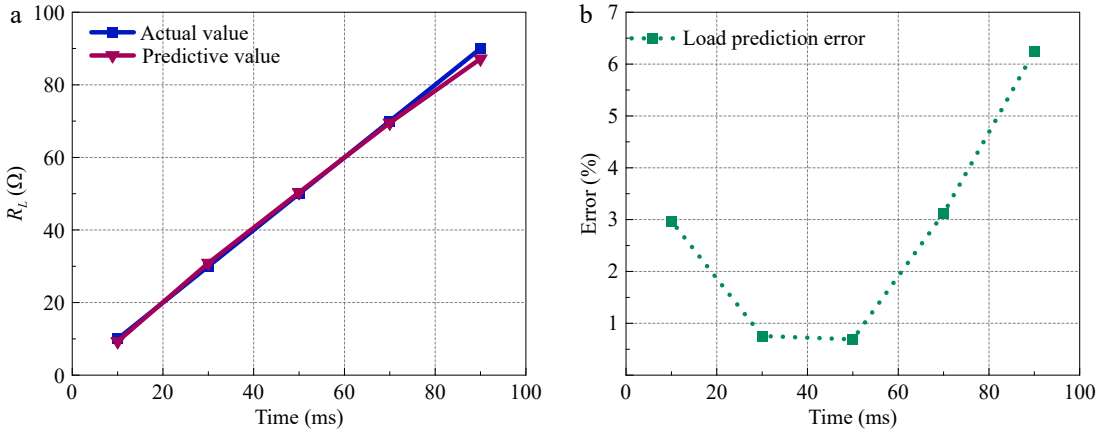

Fig. 11 Comparison of recognised values with actual values when the load changes (a) Comparison of identified and actual values. (b) Error.

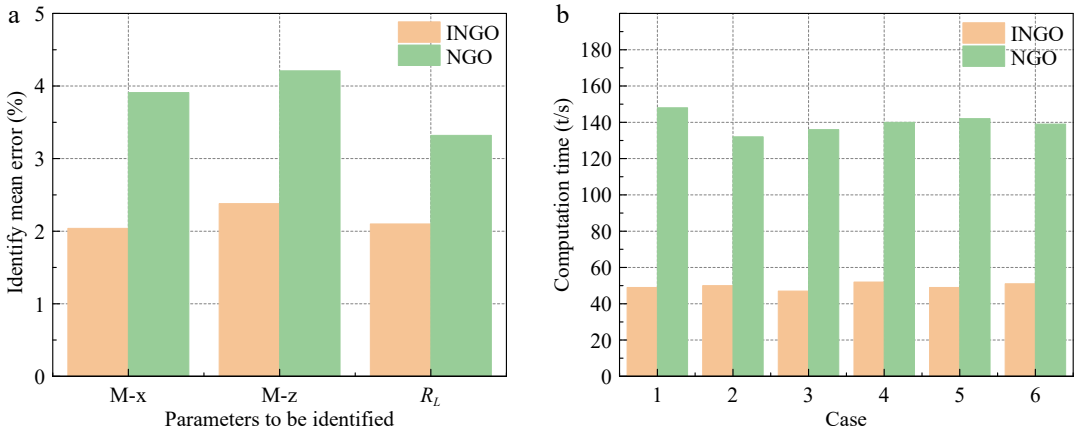

Fig. 12 Comparison of INGO and NGO algorithms. (a) Comparison of average error. (b) Comparison of computing time.

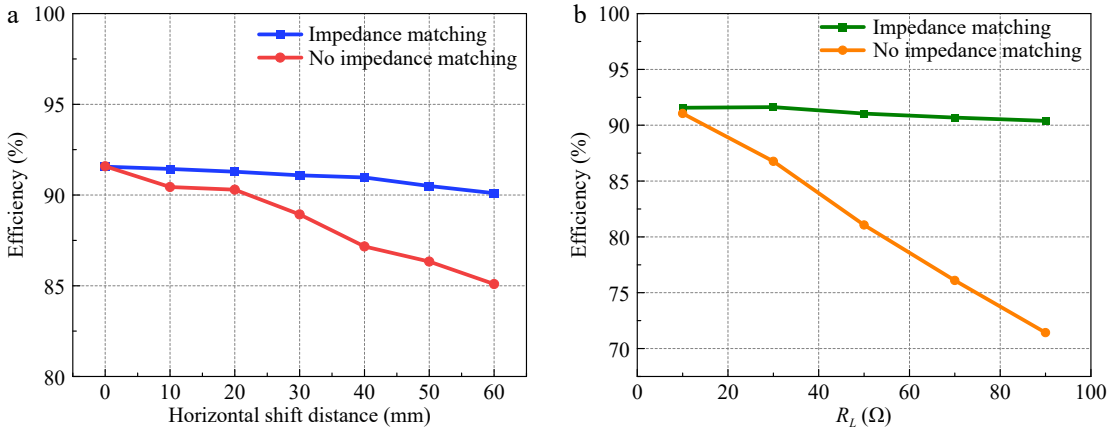

Fig. 14 Transmission efficiency with or without impedance matching applied (a) coil shift, (b) load variation.

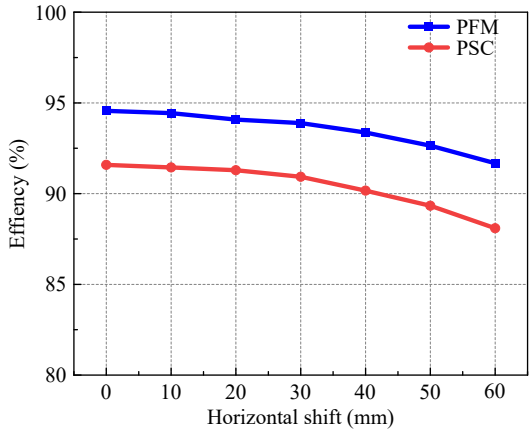

Fig. 15 Comparison of efficiency at different control strategies.

Table 7. Compared with other identification methods.

Topology	Identifiable parameters	Additional circuits	Communication	Identification error (M, R_L)	Ref.
S-S	ω, M, R_L	√	×	< 7.5%	[16]
S-S	M	√	×	< 4.8%	[17]
LCC-LCC	R_L, U_{OUT}, I_{OUT}	×	×	< 4.2%	[19]
S-S	M, L_P, L_S, C_P, C_S	×	√	< 3.0%	[27]
S-S	M, R_L	×	×	< 3.5%	This article

higher identification accuracy. Therefore, a comprehensive comparison demonstrates the superiority of the proposed method, which can also be easily adapted to different topologies by modifying the mathematical model in the algorithm.

Discussion

The experimental results validate the effectiveness of the proposed method in achieving high-precision parameter identification and maximum efficiency tracking. Compared to existing approaches, our work offers several key advancements. First, traditional methods such as those reported by Liu et al.[16] and Yang et al.[17] rely on additional circuits or complex switching operations, which increase hardware complexity and cost. In contrast, our method simplifies the system design by requiring only transmitter-side current measurements, eliminating the need for extra components. Second, the proposed INGO algorithm addresses the limitations of conventional optimization techniques by integrating an optimal value guidance strategy, a subtraction optimizer, and Cauchy mutation. These improvements enhance global convergence speed and reduce identification errors, making it particularly suitable for dynamic scenarios like EV charging where real-time adaptability is critical.

Furthermore, the PFM strategy adopted in this work overcomes the drawbacks of traditional modulation methods like PSC (high switching losses) and PDM (output fluctuations), achieving stable performance with reduced control complexity. Combined with the Sepic impedance matching circuit, our method ensures maximum efficiency tracking even under load variations and coil misalignment, as demonstrated in Fig. 14. Experimental results across diverse conditions—including horizontal/vertical offsets and load changes—confirm that the identification error remains below 3.5%, highlighting its robustness in practical applications.

While the current study focuses on SS-type topology, future work will extend this methodology to more complex topologies (e.g., LCC-LCC) and investigate environmental impacts (e.g., temperature) to broaden its applicability.

Conclusions

In this paper, a parameter identification method based on the INGO is proposed to achieve accurate identification of mutual inductance and loads between coils with lateral as well as longitudinal offsets, and by tracking the maximum efficiency of the WPT system through the identified parameters. Compared with other identification methods, algorithm identification has the advantages of reducing circuit complexity. Finally, the effectiveness of the proposed method is verified through experiments, and the experimental results show that the error of parameter identification can be kept within 3.5% by the method proposed in this paper, and the efficiency is effectively improved by the method of impedance matching.

Author contributions

The authors confirm contribution to the paper as follow: study conception and design: Guo Z, Chen S; data acquisition and data collation: Guo Z, Chen S, Zhang H, Li Z, Yu H; analysis of simulation results: Guo Z, Chen S, Nai J, Ye M; writing manuscript review & editing: Guo Z, Chen S, Tian Y; access to funds: Zhang M. All authors have read and agreed to the final version of the manuscript.

Data availability

All data generated or analyzed during this study are included in this published article.

Acknowledgments

This work was partially supported by the Natural Science Foundation of Shandong Province (Grant No. ZR2022ME214).

Conflict of interest

The authors declare that they have no conflict of interest.

Dates

Received 24 December 2024; Revised 19 February 2025; Accepted 7 March 2025; Published online 8 May 2025

References

1. Liu W, Chau KT, Tian X, Wang H, Hua Z. 2023. Smart wireless power transfer-opportunities and challenges. *Renewable & Sustainable Energy Reviews* 180:113298
2. Mi CC, Buja G, Choi SY, Rim CT. 2016. Modern advances in wireless power transfer systems for roadway powered electric vehicles. *IEEE Transactions on Industrial Electronics* 63:6533–45
3. Dai X, Jiang JC, Wu JQ. 2019. Charging area determining and power enhancement method for multiexcitation unit configuration of wirelessly dynamic charging EV system. *IEEE Transactions on Industrial Electronics* 66:4086–96
4. Jiang C, Chau KT, Liu W, Liu C, Han W, et al. 2019. An *LCC*-compensated multiple-frequency wireless motor system. *IEEE Transactions on Industrial Informatics* 15:6023–34
5. Wang H, Liu W, Chau KT. 2022. Wireless motors - a new breed of power electronics drives. *2022 IEEE 9th International Conference on Power Electronics Systems and Applications (PESA), 20-22 September 2022, Hong Kong, China*. CLP Power Hong Kong Limited; P. LEO and CO. , LTD; The Hong Kong Electric Company, Limited: Institute of Electrical and Electronics Engineers Inc. doi: 10.1109/pesa55501.2022.10038436
6. Liu W, Chau KT, Lee CHT, Cao LB, Jiang CQ. 2021. Frequency-modulated wireless direct-drive motor control. *IEEE Transactions on Magnetics* 57:8201907
7. Li Y, Hu J, Li X, Chen F, Xu Q, et al. 2020. Analysis, design, and experimental verification of a mixed high-order compensations-based WPT system with constant current outputs for driving multistring LEDs. *IEEE Transactions on Industrial Electronics* 67:203–13
8. Liu W, Chau KT, Lee CHT, Jiang C, Han W, et al. 2020. Wireless energy-on-demand using magnetic Quasi-resonant coupling. *IEEE Transactions on Power Electronics* 35:9057–69
9. Zhang Z, Chau KT, Qiu C, Liu C. 2015. Energy encryption for wireless power transfer. *IEEE Transactions on Power Electronics* 30:5237–46
10. Liu W, Chau KT, Chow CCT, Lee CHT. 2022. Wireless energy trading in traffic internet. *IEEE Transactions on Power Electronics* 37:4831–41
11. Covic GA, Boys JT. 2013. Inductive power transfer. *Proceedings of the IEEE* 101:1276–89
12. Nguyen DH. 2020. Electric vehicle - wireless charging-discharging lane decentralized peer-to-peer energy trading. *IEEE Access* 8:179616–25
13. Feng H, Cai T, Duan S, Zhang X, Hu H, et al. 2018. A dual-side-detuned series-series compensated resonant converter for wide charging region in a wireless power transfer system. *IEEE Transactions on Industrial Electronics* 65:2177–88
14. Kim M, Joo DM, Lee BK. 2019. Design and control of inductive power transfer system for electric vehicles considering wide variation of output voltage and coupling coefficient. *IEEE Transactions on Power Electronics* 34:1197–208
15. Huang Y, Shinohara N, Mitani T. 2014. A constant efficiency of rectifying circuit in an extremely wide load range. *IEEE Transactions on Microwave Theory and Techniques* 62:986–93
16. Liu C, Han W, Hu YH, Zhang BW. 2024. Simultaneous identification of multiple parameters in wireless power transfer systems using primary variable capacitors. *Applied Sciences* 14:793
17. Yang Y, Tan SC, Hui SYR. 2020. Fast hardware approach to determining mutual coupling of series-series-compensated wireless power transfer systems with active rectifiers. *IEEE Transactions on Power Electronics* 35:11026–38
18. Liu Y, Feng H. 2020. Maximum efficiency tracking control method for WPT system based on dynamic coupling coefficient identification and impedance matching network. *Ieee Journal of Emerging and Selected Topics in Power Electronics* 8:3633–43
19. Guo Y, Zhang Y, Li S, Tao C, Wang L. 2020. Load parameter joint identification of wireless power transfer system based on the DC input current and phase-shift angle. *IEEE Transactions on Power Electronics* 35:10542–53
20. Dai R, Zhou W, Chen Y, Zhu Z, Mai R. 2022. Pulse density modulation based mutual inductance and load resistance identification method for wireless power transfer system. *IEEE Transactions on Power Electronics* 37:9933–43
21. Yang JJ, Chen W. 2019. Dynamic niche artificial bee colony algorithm for output control of MCR-WPT system. *IET Microwaves Antennas & Propagation* 13:1240–47
22. Shu X, Wu G, Jiang Y. 2023. Comparative analysis of SS, SP, PP and PS topologies for magnetic coupled wireless power transfer system composed of the negative resistor. *Energies* 16:7336
23. Liu W, Chau KT, Lee CHT, Han W, Tian X, et al. 2020. Full-range soft-switching pulse frequency modulated wireless power transfer. *IEEE Transactions on Power Electronics* 35:6533–47
24. Dehghani M, Hubálovský Š, Trojovský P. 2021. Northern Goshawk optimization: a new swarm-based algorithm for solving optimization problems. *IEEE Access* 9:162059–80
25. Trojovsky P, Dehghani M. 2023. Subtraction-average-based optimizer: a new swarm-inspired metaheuristic algorithm for solving optimization problems. *Biomimetics* 8:149
26. Hua Z, Chau KT, Han W, Liu W, Ching TW. 2022. Output-controllable efficiency-optimized wireless power transfer using hybrid modulation. *IEEE Transactions on Industrial Electronics* 69:4627–36
27. Zhu G, Dong J, Grazian F, Bauer P. 2023. A parameter recognition-based impedance tuning method for SS-compensated wireless power transfer systems. *IEEE Transactions on Power Electronics* 38:13298–314